Atom probe tomography applied to the analysis of irradiated microstructures

Emmanuelle A. Marquis[a)]
Department of Materials Science and Engineering, University of Michigan, Ann Arbor, Michigan 48109, USA

(Received 28 September 2014; accepted 4 December 2014)

With its particular ability to image solute clusters in three dimensions and impurity segregation to selected interfaces and grain boundaries, atom probe tomography has provided unique insight into the effects of irradiation on materials microstructures. This article reviews the contribution of atom probe tomography to our understanding of behaviors and responses of structural materials under irradiation. Possible atom probe tomography based approaches and common data analysis methods to analyze the microstructural features often observed in irradiated materials are described. In particular, the analysis of solute clustering, solute segregation, and void imaging are discussed in the context of radiation-induced hardening of austenitic steels and reactor pressure vessel steels, and the development of oxide dispersion strengthened steels, radiation-induced solute segregation to grain boundaries for stress corrosion cracking or corrosion issues, and to understand the swelling response of irradiated materials. While highlighting the unique information that atom probe tomography can offer, common limitations, current challenges, and outstanding technical questions regarding data analysis and interpretation are also presented.

I. INTRODUCTION

Monitoring the evolution of properties of materials subjected to irradiation is a crucial aspect of nuclear safety. Irradiation can induce significant microstructural changes that have been associated with dramatic changes in properties such as fracture toughness, strength, ductility, propensity to stress corrosion cracking, or corrosion resistance.[1] Predictive models would in theory be used to ensure the appropriate selection of materials and inform on the lifetime of components by capturing the relationships between irradiation conditions imposed by specific reactor designs and resulting microstructure and property changes. Fracture toughness tests and characterization of materials retrieved from active or decommissioned plants as well as surveillance programs have indeed generated large amounts of information and knowledge regarding the behaviors of irradiated materials, and steels in particular, and informed on possible extended lifetime operation (e.g., Ref. 2). However, characterization of microstructures to a level of accuracy required for predictive models remains a challenge, in part due to the large number of variables (alloy composition, impurity levels, processing, irradiation conditions, etc.) that complicate the interpretation of the experimental data. The very small scale of the microstructural features formed in irradiated materials also stretches the limits of most characterization techniques. Despite these challenges, high-resolution characterization techniques, which include transmission electron microscopy (TEM), small angle neutron scattering (SANS), and atom probe tomography (APT), the latter being the focus of this article, have provided unique insights into the evolution of microstructures under irradiation, either in the context of failure analysis from materials retrieved from nuclear plants or in the context of laboratory scale studies, where high-energy protons or ions are often used as surrogates for neutrons.

The microstructural features induced by irradiation include, but are not limited to, solute clusters, second phases, chemistry of defect sinks, dislocation loops, and voids. Their presence in microstructures may be probed indirectly. For instance, voids affect material density, and the formation of clusters, phases, or dislocations can increase hardness. Alternatively, direct imaging of irradiated microstructures has traditionally been performed using TEM. However, the achievable chemical detectability and spatial resolution may be challenged by the nanometer scale dimensions of solute clusters, low levels of solute segregation, or segregation of impurities such as C. In addition, for very complex microstructures, the analysis and interpretation of TEM images taken from thin foils containing high number densities of solute clusters, nanoscale precipitates, and small dislocation loops can become nontrivial. SANS, which also is often used to characterize irradiated microstructures (e.g., Ref. 3), requires some prior knowledge and assumptions regarding the features being analyzed to interpret the data. Instead, APT fills the gap left by the

Contributing Editor: Joel Ribis
[a)]Address all correspondence to this author.
e-mail: emarq@umich.edu
DOI: 10.1557/jmr.2014.398

 © Materials Research Society 2014

https://doi.org/10.1557/jmr.2014.398 Published online by Cambridge University Press

other experimental techniques with its ability to directly image atoms and therefore local chemistry in three dimensions. APT combines time-of-flight mass spectrometry and position-sensitive detection to analyze ionized atoms that are field-evaporated from needle-shaped specimens. Each detected ion is positioned within a volume, which can be constructed and scaled based on, for instance, an inferred or measured specimen geometry, known crystallographic orientation and plane spacing, a simple projection law between the specimen and the detector,[4] or on some known geometrical characteristic of the microstructure (precipitate shape, size, grain boundary position, etc.). Examples of different reconstruction approaches can be found in Ref. 5. Depending on the instrumentation used, between 30 and 90% of the atoms are detected, chemically identified, and positioned with an accuracy which depends on the analyzed material, the local crystallographic orientation with the specimen, the selected microstructure, the relative position of the features within the microstructure and within the specimen, evaporation conditions, sample geometry, and the selected reconstruction algorithm. It can therefore vary between a few angstroms to a few nanometers within the same dataset. More details on the principles of the APT technique can be found in the existing review articles and books (e.g., Refs. 6 and 7). For neutron-irradiated materials with significant background radiation, the use of focused ion beam (FIB) milling to reduce the volumes of material required to prepare and perform APT analyses has significantly facilitated the adoption of APT as a major characterization technique for irradiated materials.

This article focuses on three types of microstructural features found in irradiated materials: solute clusters, solute segregation to grain boundaries, and voids. First, the ability of APT to resolve solute clusters has motivated its use in the characterization of irradiated steels currently used in reactors and in the development of oxide dispersion strengthened (ODS) steels. The selected examples highlight strengths and limitations of the APT technique in addressing the quantification of solute clusters. Because radiation-induced segregation plays a significant role among all radiation degradation phenomena, a summary of possible approaches to perform quantitative analyses of solute and impurity segregation to grain boundaries is then presented. These measurements benefit from the chemical sensitivity of APT that is theoretically constant across the periodic table and is better than that typically achievable with analytical TEM methods for common impurity elements, while other techniques with better chemical sensitivity, such as SIMS, lack the spatial resolution. In addition, quantification does not require the use of standards, and the recently developed methods for analyzing crystallographic information present in the APT dataset. To finish, visualization and analysis of voids using APT are briefly reviewed.

II. INSIGHTS INTO SOLUTE CLUSTERING

APT has been instrumental in the analysis of solute clustering that would not be directly imaged and quantified by other characterization techniques. However, quantifying the size, number density, and chemistry of solute clusters is not necessarily a straightforward task. Rather, the analysis of solute clustering is an ongoing research topic that involves understanding inherent technique artifacts, developing correction methods and data analysis procedures, and quantifying uncertainties and errors. Commonly observed artifacts include trajectory aberrations,[8] evaporation of several ions on the same voltage or laser pulse that may not be detected,[9,10] and preferential evaporation or retention of certain solute elements over others leading to biased detection and erroneous compositions.[11] The particular artifact of trajectory aberrations traditionally refers to the presence of defects or different phases with different evaporation fields at the specimen surface. The variations in evaporation field over the surface lead to local variations in the surface curvature. Since ion trajectories are controlled by the field distribution over the surface, a nonuniform surface curvature yields nonuniform projection[8] and in worse cases crossing of ion trajectories. It is therefore obvious that data reconstructions assuming a spherical specimen end shape may contain significant positioning artifacts.[8,12] Additional examples of artifacts will be discussed throughout the article.

The different data analysis methods that have been applied to the analysis of solute clustering have been reviewed elsewhere.[13] However, the main approach to quantifying solute clustering is based on the concept of a maximum separation distance, d_{max}; two or more atoms are part of the same cluster if they are all positioned within a sphere of radius d_{max}.[14,15] Additional parameters, such as inclusion and erosion distances[14] or order parameter,[15] can be selected to refine cluster definitions and define cluster compositions. We note that the results of this analysis method are highly sensitive to the selection of the input parameters, which, unfortunately, the published literature does not always make clear. Limitations of the method and variability of the measured cluster sizes, number densities, and composition on the chosen values are rarely discussed.[16] Other exceptions include Styman et al.[17] and Williams et al.[18] for their analyses of solute clusters in reactor pressure vessel (RPV) and ODS steels.

The motivation in using APT to quantify size and number density of various solute clusters found in irradiated RPV steels came from the need to assess their hardening effects and therefore to develop empirical relationships between microstructure and hardening that

https://doi.org/10.1557/jmr.2014.398 Published online by Cambridge University Press

could be extrapolated to relationships between irradiation condition and embrittlement without having to go through an expensive campaign of materials testing. The presence of small clusters of Ni, Mn, and Cu in irradiated steel welds was shown directly for the first time using atom probe field ion microscopy (APFIM), an older version of the APT technique.[19] Since, APT has been used to quantify irradiation-induced solute clusters in various steels retrieved from nuclear reactors. Overall, it was determined that the presence of Cu is particularly deleterious through the formation of CuMnNi clusters. APT has uniquely revealed the formation of solute clusters, with a strong effect of dose and impurity content on their formation, size, and number density (e.g., Ref. 20). APT also played a key role in the selection of annealing treatments of plant steels used to recover the hardening effect generated by the formation of small clusters.[21] In low Cu steels, Odette also predicted the appearance of other types of clusters, specifically NiMnSi clusters or "late blooming phases", forming at high fluences and leading to significant embrittlement.[22] Experimental evidence from APT analyses exists for such NiMnSi clusters formed in irradiated steels[23] or in thermally annealed steels[24] and Wells et al.[25] recently showed that a high volume fraction of Mn–Ni–Si phase form in Cu-free and Cu-bearing steels irradiated at high fluence.[25] In their analysis of the small clusters, Wells et al.[25] highlighted the importance of considering local composition (as opposed to the alloy composition) when analyzing precipitate data.

As a side note, significant discussions within the APT and SANS communities were generated over the question of the possible presence of Fe in the Cu clusters. SANS data analyzed using experimental magnetization data at room temperature showed that almost pure Cu precipitates are formed[26] contrasting with early APT work reporting Fe concentrations in Cu clusters in the range of 27–52%.[27] Odette et al.[26] suggested that some of the detected Fe atoms originate from trajectory aberrations and Morley et al.[28] showed that the detected concentrations of Fe within Cu precipitates could reduce to $<5\%$ when taking into account these artifacts. Trajectory aberrations leading to a spatial overlap between matrix and cluster ions and a potential dilution of cluster compositions are not specific to the analysis of Cu clusters in Fe. Similar observations are described below for the detection of Fe inside oxide nanoclusters in ODS steels. The same question can be extended to the observed Fe content in nanoscale Cr-rich α' precipitates formed in neutron irradiated Fe–Cr based steels and analyzed by APT (e.g., Refs. 29 and 30).

Similar to RPV steels, irradiated 304 steels exhibit a number of irradiation-induced features, which include the formation of Cu clusters, Ni/Si clusters, Ni_3Si, and G-phase precipitates. In proton-irradiated 304 in particular, the very high number density of features formed and their spatial interactions make the microstructure extremely complex. Yet, APT has been instrumental in resolving the spatial arrangement of the different features (dislocations with solute segregation, clusters along dislocations, or clusters in the matrix). We note that the maximum separation method was originally developed for the analysis of clusters with high concentrations of solutes forming in dilute matrices. Its application to the analysis of proton-irradiated 304 microstructures, where different types of clusters involve the same solute species, the interface between clusters and matrix is broad, and the compositional difference between matrix and clusters is not large, may lead to inaccurate interpretations. To address this issue, Chen et al.[31] developed a procedure for optimizing the selection of cluster parameters in an effort to provide a systematic and quantitative analysis of the microstructures. As an illustration, the method can resolve Ni-rich clusters along a Ni and Si segregated dislocation loop in a proton implanted 304 steel [Fig. 1(a)]. APT also provides a quick approach to compare different irradiation methods. For instance, significantly different microstructures are observed in 304 steels neutron-irradiated at low dose rates where larger and fewer Ni and Si segregated dislocation loops and larger Ni_3Si precipitates are observed, as illustrated in Fig. 1(b). The local composition analysis also revealed that the clusters are

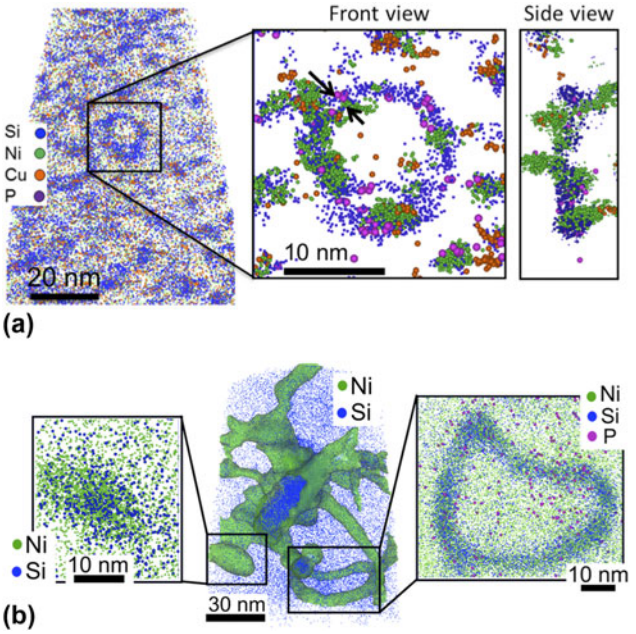


FIG. 1. (a) Slice taken from a reconstructed APT volume revealing Cu, Ni, and Si clustering and Ni, Si, and P segregation to dislocation loops in a 304 proton implanted to 10 dpa at 360 °C (from Ref. 31). (b) Reconstructed APT volume from a 304 steel neutron irradiated at 450 °C to 28 dpa revealing large Ni and Si segregated dislocation loops as well as large Ni_3Si precipitates (data courtesy of Y. Dong, University of Michigan).

https://doi.org/10.1557/jmr.2014.398 Published online by Cambridge University Press

Mn-depleted under proton irradiation but Mn-enriched under neutron irradiation.

The search for radiation tolerant materials has focused significant effort on the development of ODS steels, which contain high densities of nanometer scale yttrium-rich oxide particles or nanoclusters. It is thought that the nanocluster interfaces might act as sinks for point defects, thereby mitigating void swelling.[32] Optimization of the radiation resistance of ODS steels would require some knowledge of the oxide particles forming during processing as well as an understanding of their behavior under irradiation. Larson et al.[33] performed the first APT analyses, followed by Miller et al.[27,34,35] on a Fe–14Cr containing W, Ti, and Y. A number of studies followed with APT analyses of different ODS steels (e.g., Refs. 36–39). Most of the debate regarding these APT analyses has revolved around the question of the measured composition of the nanoclusters. It appears that differing interpretations often originated from discrepancies and uncertainties in the methods used to analyze the data, which were not necessarily described in the published literature. While the expected stoichiometry is measured for the larger particles (>10 nm),[39] the reported cluster compositions often are significantly oxygen and yttrium deficient for the smaller particles. The measured compositions also suggest significant amounts of Fe within the nanoclusters, which for the most part, if not entirely, may be the result of trajectory aberrations. Indeed, the dark contrast at the particle locations observed by field ion microscopy[40] and the high density of matrix ions reconstructed at the particle locations[41] are consistent with the oxide particles having a lower evaporation field than that of the Fe-rich matrix [Fig. 2(c)]. This difference of evaporation field would in turn lead to trajectory aberrations. Other observed artifacts relate to oxygen migration, either on the evaporating surface of the specimens leading to an apparent spread of the oxygen atoms around the nanoclusters, or in depth due to field-induced migration followed by molecular evaporation with atoms still present on the surface [Fig. 2(b)]. This particular effect has been observed during field evaporation of different oxide/metal systems and can result in a false oxide layer reconstructed at the oxide/metal interface.[42] Bypassing the question of the origin of the Fe observed within the clusters, Williams et al.[43] proposed to subtract the Fe content and the corresponding amount of solute elements in proportion to the matrix composition – a method that would allow quantitative comparison of the oxide clusters between different alloys, processing routes, or irradiation conditions. Understanding the raw data and detector limitations is also important to quantify measurement errors and interpret the observed compositions.[18] The inhomogeneous spatial distributions of nanoclusters very often found in ODS alloys present an additional challenge for APT analyses only able to capture volumes smaller than the length scale of the spatial inhomogeneity. This is addressed by complementing the analyses with TEM observations. Despite these challenges, APT has offered unique information regarding the structure, composition, and irradiation behavior of ODS steels. A core–shell structure was unambiguously observed around oxide particles in ODS steels of different compositions,[40] in agreement with prior TEM observations.[44] The irradiation behavior of ODS steels has also been the object of great interest and a number of APT studies. Somewhat contradictory findings have been reported in the literature, e.g., dissolution of the nanoclusters[45] versus particle coarsening,[46] which may be resolved by considering the temperature at which irradiations were performed and therefore the balance between mixing and reprecipitation.[45]

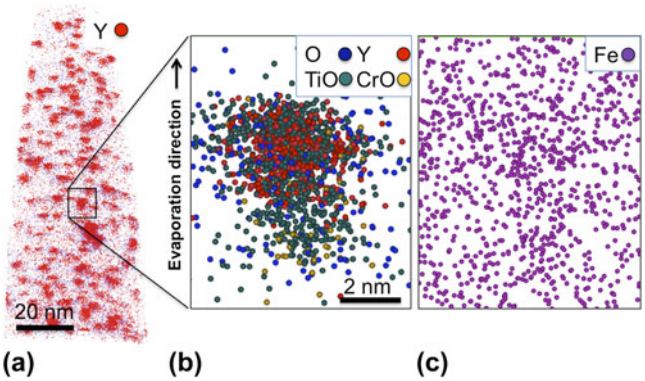


FIG. 2. (a) APT reconstruction showing the distribution of oxide nanoclusters identified by the high density of Y and YO ions. (b) A 7 nm thick slice through one nanocluster illustrates the observed spatial distribution of the different identified ions. (c) The Fe spatial distribution is shown in a 3 nm thick slice where a slightly higher density of Fe is observed at the location of the nanocluster (data courtesy of Y. Chen, University of Michigan).

Finally, APT is not only used to characterize multicomponent industrial steels but can also be used to answer basic scientific questions regarding the irradiation behavior of alloys. A recent example illustrating this approach focuses on the quantification of α′ precipitation in a series of model Fe–Cr alloys. The use of neutron irradiation at different temperatures and doses combined with thermal annealing is currently being used to validate the theoretically predicted Fe–Cr phase diagram,[30] and to quantify precipitation and diffusion kinetics, and the effect of irradiation on the chemistry of grain boundaries. As an illustration, the different microstructures obtained in the series of alloys for the same irradiation condition are shown in Fig. 3. Size, number density, and chemistry of α′ precipitates were quantified using the methods described above.[30]

To summarize, provided that potential artifacts related to the APT technique are understood and taken into account, APT provides a quantitative approach to

https://doi.org/10.1557/jmr.2014.398 Published online by Cambridge University Press

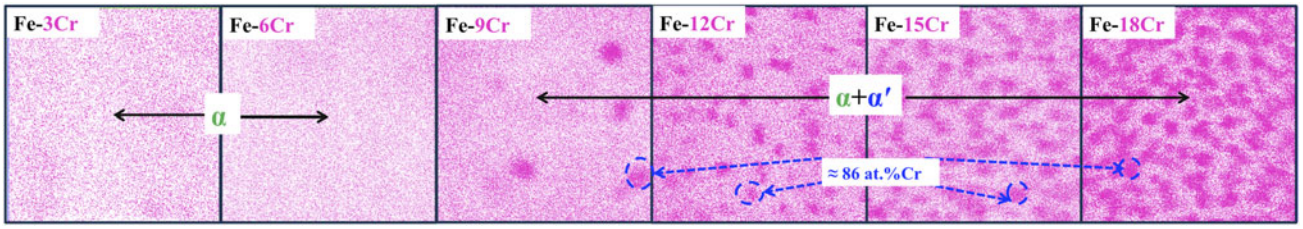


FIG. 3. Thin slices extracted from larger APT reconstructions that were obtained from a series of Fe–Cr alloys containing from 3 to 18 at.% Cr and neutron irradiated at 280 °C to 1.8 dpa. The presence of α′ clusters is observed for Cr concentration above 9 at.% indicating that the solubility limit for Cr in Fe is below this concentration. Size, number density, and concentration measurements are reported in Ref. 30.

measuring sizes, number densities, and compositions of nanometer scale solute clusters formed in irradiated alloys. It is important that APT analyses be compared to TEM observations or SANS measurements for consistency. While unique in providing 3D chemical mapping, APT is limited in the amount of local structural information; therefore, interpretation of APT data can significantly benefit from TEM observations. The selected examples illustrate how analysis and filtering methods can be developed to analyze complex distributions of features within a microstructure providing quantitative information that may ultimately be used for mechanical property and materials behavior predictions. The development of such robust methods able to distinguish and separate these different features remains an open research topic. In-depth raw data analyses, future detector improvement, and correlative work using complementary techniques such as TEM and electron energy loss spectrometry (EELS)[47] will clarify some of the open questions and ambiguities regarding potential loss of detected ions during APT analysis, solute cluster or oxide nanocluster compositions, and ultimately their behaviors under irradiation.

III. SOLUTE SEGREGATION

Radiation-induced segregation (RIS) of solute atoms at grain boundaries is a concern when it affects materials properties such as susceptibility to stress corrosion cracking. However, changes in the chemistry of grain boundaries observed after irradiation may originate from different mechanisms. Irradiation can induce faster diffusion by the presence of high densities of point defects, and nonequilibrium distributions of solutes leading to segregation at grain boundaries or dislocations, which would otherwise not be observed under thermal equilibrium conditions. Unambiguously, determining the controlling mechanism may be difficult in some cases. In addition, the formation of carbides or nitride phases at grain boundaries can, in some instances, also affect the chemistry of neighboring grain boundaries and lead to Cr depletion and consequently stress corrosion susceptibility and corrosion, a phenomenon also known as sensitization.[48] In analyzing grain boundary segregation, one has to therefore question (1) the representative character of the analysis – is the chosen grain boundary relevant for the property considered and would it change if a different boundary was analyzed; (2) the variability and reproducibility of the analysis – is the measurement dependent on the location along the grain boundary and on the methods by which it was collected and analyzed; and (3) whether the observation is a manifestation of an irradiation-related phenomenon or a consequence of the surrounding microstructure.

Since grain boundary energy is a function of grain boundary orientation, segregation under thermal equilibrium is also expected to be a function of grain boundary orientation.[49] For irradiated steels, the grain boundary response depends on its sink strength or the ability to absorb point defects, which has been shown to be a function of the grain boundary structure and therefore orientation.[50] Therefore when quantifying solute segregation, the distinction between prior austenite grain boundaries and lath boundaries in ferritic martensitic steels or between large angle grain boundaries or twin boundaries in austenitic steels is often performed. Grain boundaries may be selected and specimens prepared based on prior scanning electron microscopy (SEM) imaging or electron backscattered diffraction (EBSD) analysis of the surface (e.g., Refs. 51–53). Grain boundary information can also be obtained by imaging the APT specimens by TEM prior to APT analysis.[54] More recent tools developed to extract crystallographic information from APT datasets can, in some cases, also reveal grain orientation and therefore information on grain boundary misorientation without having to rely on SEM, EBSD, or TEM analysis (e.g., Refs. 55 and 56).

Segregation measurements are often obtained from one-dimensional concentration profiles calculated along small volumes positioned orthogonal to the boundary plane. Recent methods have also been developed to consider the entire boundary surface captured within the dataset.[57] Because of the resolution anisotropy inherent to APT data, the observed segregation profiles

https://doi.org/10.1557/jmr.2014.398 Published online by Cambridge University Press

for a boundary orthogonal to the specimen axis are expected to be sharper than if the boundary is positioned parallel to the tip axis. The height of the segregation peak may therefore not be of much relevance as it depends on the orientation of the grain boundary plane within the APT specimen.[58] Instead most studies report excess values that can be calculated from area under the segregation or depletion peak in a concentration profile (e.g., Ref. 59). For such an interfacial segregation analysis that also relies on a measurement of the matrix concentration, any crystallographic artifacts resulting in local variations of solute concentrations should be considered carefully. The preferential retention and preferential evaporation of specific species between voltage or laser pulses (DC evaporation) have been discussed in a number of studies (e.g., Ref. 11). Surface migration of solute atoms or impurities, such as Si, C, P, or N in steels, also results in a crystallographic dependence of the measured composition, as discussed in Ref. 60 and illustrated in Fig. 4(b). Beyond these preliminary steps required to analyze the APT data, many examples of measurements of grain boundary chemistry in irradiated materials using APT can be found in the literature (e.g., Refs. 61–64).

Dislocations can, in most cases, be observed only if solute segregation is present. Several examples of solute segregation to dislocations can be found in the literature (e.g., Refs. 31, 65, and 66). One might note, however, that the APT specimens during analysis are subjected to large mechanical stresses and possibly non-negligible temperature rises when using laser pulsing that may lead to migration of some defects. While solute segregation tends to pin dislocations, it would be recommended to perform complementary analyses (e.g., TEM imaging of APT specimens before and after APT analysis or of thin foils) to verify the integrity of the features of interest during field evaporation. Nonetheless, in many cases, careful data analysis has led to the quantification of dislocation segregation and line density. Figure 1 also illustrates the possible analysis of heterogeneous nucleation of solute clusters along dislocation loops. The analysis of the crystallographic orientation of the samples using desorption patterns offers additional information on the nature of the dislocations. For instance, Bachhav et al.[52] determined the habit planes of dislocation loops in a neutron irradiated Fe–Cr alloy, which is an indirect observation of the dislocation Burger's vectors (Fig. 5). This approach is complementary to the more common Burger's vector analysis from TEM foils. Another successful approach was provided by Bhattacharya et al.[67] who analyzed the distribution of Cr atoms within dislocation loops formed in Fe–Cr

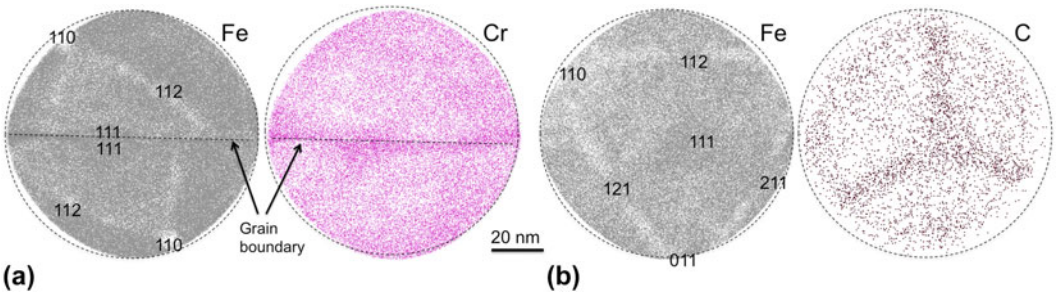


FIG. 4. (a) Thin slices showing representative cumulative desorption maps of Fe and Cr with clear crystallographic directions. A Σ3 grain boundary revealed by the locally higher Cr density runs through the analysis. (b) Cumulative desorption maps of Fe and C for a different specimen illustrating the crystallographic dependence of C evaporation (data courtesy of M. Bachhav, University of Michigan).

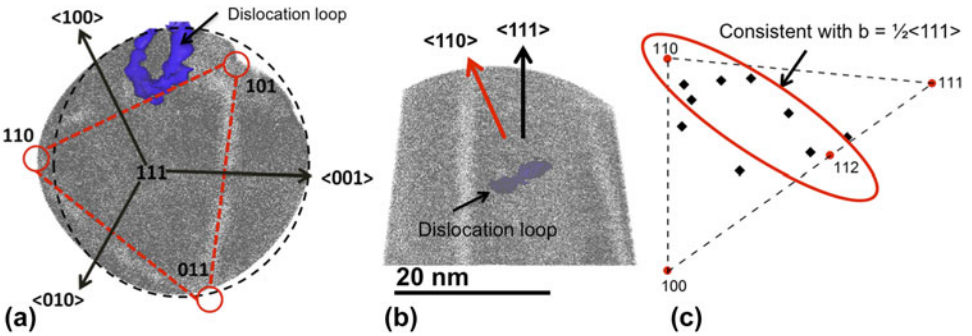


FIG. 5. Dislocation analysis in a neutron irradiated Fe–6Cr alloy using the crystallographic information available from the desorption map (top view) to inform on the normal direction to the dislocation habit plane (side view). From the habit plane orientation, all dislocation loops analyzed are consistent with ½<111> type loops (data courtesy of M. Bachhav and L. Yao, University of Michigan).

https://doi.org/10.1557/jmr.2014.398 Published online by Cambridge University Press

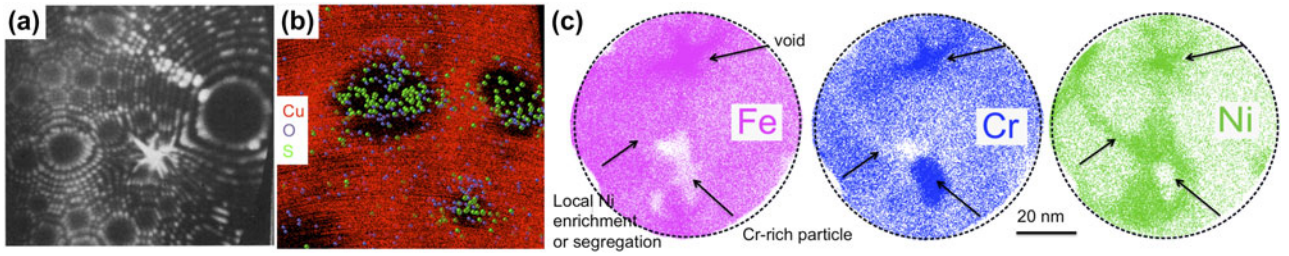


FIG. 6. (a) FIM image showing a star-like pattern for voids formed in a W filament (reproduced from Ref. 69). (b) Slice through a reconstructed APT volume showing voids in an ODS steel (reproduced from Ref. 70). (c) Cumulative desorption maps of Fe, Cr, and Ni showing the presence of a void by the star-shaped high ion density region that can be clearly distinguished from the other microstructural features (data courtesy of Y. Dong, University of Michigan).

alloys by using TEM for orientation and chemical analysis complemented by APT imaging for the 3D information of the Cr distribution within the loop.

IV. ANALYSIS OF VOIDS

Small voids or bubbles have previously been imaged by field ion microscopy (FIM) and APT. The observed patterns by FIM vary from local distortions of the surface atomic structure[68] to high intensity star-like patterns,[69,70] as illustrated in Fig. 6(a) reproduced from Ref. 69. The observed image and high intensity associated with the presence of voids were qualitatively explained by modeling of the field distribution over the evaporating surface containing a small cavity at the surface of the specimen[71] and explained by trajectory aberrations of the field-desorbed ions at the void edges.[70,72] High density patterns have also been observed in APT datasets obtained from neutron irradiated steels for which TEM has shown the presence of nanometer size voids. An example is shown in Fig. 6(c) where the star-shaped density patterns of all major matrix elements (Fe, Cr, and Ni) resemble that observed in the FIM image shown in Fig. 6(a). Again the apparent high density is attributed to ion trajectory aberrations induced by the dramatic change in curvature at the edge of the void. Recently published APT data indicate that voids or bubbles may also be reconstructed as cavities,[72] as illustrated in Fig. 6(b) reproduced from Ref. 70. Further analyses will clarify the origin of these different patterns.

V. CONCLUSIONS

This article highlighted possibilities, current limitations, and common methods for analyzing irradiated microstructures. It is believed that future efforts in standardization, detailed and complete reports of experimental protocols in peer-reviewed publications, and further quantification of errors and uncertainties will contribute to ensure that APT data are considered reliable and reproducible. In addition, continued developments in data analysis and the use of APT with complementary techniques such as discussed in Ref. 73 for the combined use of APT and SANS, or use within larger multiscale approaches (e.g., Ref. 74), will uniquely contribute to a deeper understanding of materials behavior under irradiation.

ACKNOWLEDGMENT

The author would like to acknowledge financial support from the DOE Office of Nuclear Energy's Nuclear Energy University Programs at the University of Michigan.

REFERENCES

1. S.J. Zinkle and J.T. Busby: Structural materials for fission and fusion energy. *Mater. Today* **12**, 12–19 (2009).
2. R.K. Nanstad, R.E. Stoller, M.K. Miller, and M.A. Sokolov: In-service degradation and life extension of nuclear reactor vessels: Combining experiments and modelling. In *Proceedings of the First International Conference on Ageing Studies and Lifetime Extension of Materials*, L.G. Mallison ed.; Kluwer Academic/Plenum Publishers: New York, Oxford, 2001; pp. 565–582.
3. M.A. Sokolov, K.C. Littrell, and R.K. Nanstad: *Reactor Pressure Vessel Task of Light Water Reactor Sustainability Program: Milestone M3LW-13OR0402012, Report on Small-Angle Neutron Scattering Experiments of Irradiated RPV Materials* (Oak Ridge National Laboratory, 2012).
4. A. Cerezo, P.J. Warren, and G.D.W. Smith: Some aspects of image projection in the field-ion microscope. *Ultramicroscopy* **79**, 251–257 (1999).
5. F. Vurpillot, B. Gault, B.P. Geiser, and D.J. Larson: Reconstructing atom probe data: A review. *Ultramicroscopy* **132**, 19–30 (2013).
6. T.F. Kelly and M.K. Miller: Invited review article: Atom probe tomography. *Rev. Sci. Instrum.* **78**, 031101 (2007).
7. B. Gault, M.P. Moody, J.M. Cairney, and S.P. Ringer: *Atom Probe Microscopy* (Springer, 2012).
8. M.K. Miller and M.G. Hetherington: Local magnification effects in the atom probe. *Surf. Sci.* **246**, 442–449 (1991).
9. F. De Geuser, B. Gault, A. Bostel, and F. Vurpillot: Correlated field evaporation as seen by atom probe tomography. *Surf. Sci.* **601**, 536–543 (2007).
10. G. Da Costa, H. Wang, S. Duguay, A. Bostel, D. Blavette, and B. Deconihout: Advance in multi-hit detection and quantization in atom probe tomography. *Rev. Sci. Instrum.* **83**, 123709 (2012).

https://doi.org/10.1557/jmr.2014.398 Published online by Cambridge University Press

11. M.K. Miller and G.D.W. Smith: An atom probe study of the anomalous evaporation of alloys containing Si. *Ultramicroscopy* **5**, 238–239 (1980).
12. E.A. Marquis, B.P. Geiser, T.J. Prosa, and D.J. Larson: Evolution of tip shape during field evaporation of complex multilayer structures. *J. Microsc.* **241**, 225–233 (2011).
13. E.A. Marquis and J.M. Hyde: Applications of atom-probe tomography to the characterisation of solute behaviours. *Mater. Sci. Eng., R* **69**, 37–62 (2010).
14. D. Vaumousse, A. Cerezo, and P.J. Warren: A procedure for quantification of precipitates microstructures from three-dimensional atom probe data. *Ultramicroscopy* **95**, 215–221 (2003).
15. L.T. Stephenson, M.P. Moody, P.V. Liddicoat, and S.P. Ringer: New techniques for the analysis of fine-scaled clustering phenomena within atom probe tomography (APT) data. *Microsc. Microanal.* **13**, 448–463 (2007).
16. A. Cerezo and L. Davin: Aspects of the observation of clusters in the 3-dimensional atom probe. *Surf. Interface Anal.* **39**, 184–188 (2007).
17. P.D. Styman, J.M. Hyde, K. Wilford, and G.D.W. Smith: Quantitative methods for the APT analysis of thermally aged RPV steels. *Ultramicroscopy* **132**, 258–264 (2013).
18. C.A. Williams, D. Haley, E.A. Marquis, G.D.W. Smith, and M.P. Moody: Defining clusters in APT reconstructions of ODS steels. *Ultramicroscopy* **132**, 271–278 (2012).
19. M.G. Burke and S.S. Brenner: Microstructural investigation of irradiated pressure vessel steel weld metal. *J. Phys. Colloques* **47**, 239–244 (1986).
20. M.K. Miller, R.K. Nanstad, M.A. Sokolov, and K.F. Russell: The effects of irradiation, annealing and reirradiation on RPV steels. *J. Nucl. Mater.* **351**, 216–222 (2006).
21. P. Auger, P. Pareige, S. Welzel, and J.C. Van Duysen: Synthesis of atom probe experiments on irradiation-induced solute segregation in French ferritic pressure vessel steels. *J. Nucl. Mater.* **280**, 331–344 (2000).
22. G.R. Odette: Radiation induced microstructural evolution in reactor pressure vessel steels. *MRS Symp.* **373**, 137 (1995).
23. M.K. Miller, K.A. Powers, R.K. Nanstad, and P. Efsing: Atom probe tomography characterizations of high nickel, low copper surveillance RPV welds irradiated to high fluences. *J. Nucl. Mater.* **437**, 107–115 (2013).
24. P.D. Styman, J.M. Hyde, K. Wilford, A. Morley, and G.D.W. Smith: Precipitation in long term thermally aged high copper, high nickel model RPV steel welds. *Prog. Nucl. Energy* **57**, 86–92 (2012).
25. P. Wells, T. Yamamoto, M.B.T. Milot, J. Cole, Y. Wu, and G.R. Odette: Evolution of manganese–nickel–silicon-dominated phases in highly irradiated reactor pressure vessel steels. *Acta Mater.* **80**, 205–219 (2014).
26. G.R. Odette, C.L. Liu, and B.D. Wirth: On the composition and structure of nanoprecipitates in irradiated pressure vessel steels. *Mater. Res. Soc. Symp. Proc.* **439**, 457 (1997).
27. M.K. Miller, B.D. Wirth, and G.R. Odette: Precipitation in neutron-irradiated Fe–Cu and Fe–Cu–Mn model alloys: A comparison of APT and SANS data. *Mater. Sci. Eng., A* **353**, 133–139 (2003).
28. A. Morley, G. Sha, S. Hirosawa, A. Cerezo, and G.D.W. Smith: Determining the composition of small features in atom probe: bcc Cu-rich precipitates in an Fe-rich matrix. *Ultramicroscopy* **109**, 535–540 (2009).
29. S. Novy, P. Pareige, and C. Pareige: Atomic scale analysis and phase separation understanding in a thermally aged Fe–20 at.%Cr alloy. *J. Nucl. Mater.* **384**, 96–102 (2009).
30. M. Bachhav, G. Robert Odette, and E.A. Marquis: α' precipitation in neutron-irradiated Fe–Cr alloys. *Scr. Mater.* **74**, 48–51 (2014).
31. Y. Chen, P.H. Chou, and E.A. Marquis: Quantitative atom probe tomography characterization of microstructures in a proton irradiated 304 stainless steel. *J. Nucl. Mater.* **451**, 130–136 (2014).
32. G.R. Odette, M.J. Alinger, and B.D. Wirth: Recent developments in irradiation-resistant steels. *Annu. Rev. Mater. Res.* **38**, 471–503 (2008).
33. D.J. Larson, P.J. Maziasz, I.S. Kim, and K. Miyahara: Three-dimensional atom probe observation of nanoscale titanium-oxygen clustering in an oxide-dispersion-strengthened Fe-12Cr-3W-0.4Ti+Y_2O_3 ferritic alloy. *Scr. Mater.* **44**, 359–364 (2001).
34. M.K. Miller, E.A. Kenik, K.F. Russell, L. Heatherly, D.T. Hoelzer, and P.J. Maziasz: Atom probe tomography of nanoscale particles in ODS ferritic alloys. *Mater. Sci. Eng. A* **353**, 140–145 (2003).
35. M.K. Miller, K.F. Russell, and D.T. Hoelzer: Characterization of precipitates in MA/ODS ferritic alloys. *J. Nucl. Mater.* **351**, 261–268 (2006).
36. M. Brocq, B. Radiguet, J.M. Le Breton, F. Cuvilly, P. Pareige, and F. Legendre: Nanoscale characterisation and clustering mechanism in an Fe-Y_2O_3 model ODS alloy processed by reactive ball milling and annealing. *Acta Mater.* **58**, 1806–1814 (2010).
37. A. Etienne, N.J. Cunningham, Y. Wu, and G.R. Odette: Effects of friction stir welding and post-weld annealing on nanostructured ferritic alloy. *Mater. Sci. Technol.* **27**, 724–728 (2011).
38. A.G. Certain, K.G. Field, T.R. Allen, M.K. Miller, J. Bentley, and J.T. Busby: Response of nanoclusters in a 9Cr ODS steel to 1 dpa, 525 degrees C proton irradiation. *J. Nucl. Mater.* **407**, 2–9 (2010).
39. C.A. Williams, G.D.W. Smith, and E.A. Marquis: The effect of Ti on the coarsening behavior of oxygen-rich nanoparticles in oxide-dispersion-strengthened steels after annealing at 1200 degrees C. *Scr. Mater.* **67**, 108–111 (2012).
40. E.A. Marquis: Core/shell structures of oxygen-rich nanofeatures in oxide-dispersion strengthened Fe-Cr alloys. *Appl. Phys. Lett.* **93**, (2008).
41. P. Wells, N.J. Cunningham, and G.R. Odette: Recent progress on understanding and quantifying atom probe tomography artifacts for high evaporation rate nm-scale phases in Fe based alloys. In DOE/ER-0313/51, ed. *Fusion Reactor Materials Program2011*. pp. 9–21.
42. D.J. Larson, E.A. Marquis, P.M. Rice, T.J. Prosa, B.P. Geiser, S.H. Yang, and S.S.P. Parkin: Manganese diffusion in annealed magnetic tunnel junctions with MgO tunnel barriers. *Scr. Mater.* **64**, 673–676 (2011).
43. C.A. Williams, E.A. Marquis, A. Cerezo, and G.D.W. Smith: Nanoscale characterisation of ODS-Eurofer 97 steel: An atom-probe tomography study. *J. Nucl. Mater.* **400**, 37–45 (2010).
44. M. Klimenkov, R. Lindau, and A. Moslang: New insights into the structure of ODS particles in the ODS-Eurofer alloy. *J. Nucl. Mater.* **386**, 553–556 (2009).
45. A. Certain, S. Kuchibhatla, V. Shutthanandan, D.T. Hoelzer, and T.R. Allen: Radiation stability of nanoclusters in nano-structured oxide dispersion strengthened (ODS) steels. *J. Nucl. Mater.* **434**, 311–321 (2013).
46. M.L. Lescoat, J. Ribis, Y. Chen, E.A. Marquis, E. Bordas, P. Trocellier, Y. Serruys, A. Gentils, O. Kaïtasov, Y. de Carlan, and A. Legris: Radiation-induced Ostwald ripening in oxide dispersion strengthened ferritic steels irradiated at high ion dose. *Acta Mater.* **78**, 328–340 (2014).
47. A.J. London, S. Lozano-Perez, S. Santra, S. Amirthapandian, B.K. Panigrahi, C.S. Sundar, and C.R.M. Grovenor: Comparison of atom probe tomography and transmission electron microscopy analysis of oxide dispersion strengthened steels. *J. Phys.: Conf. Ser.* **522**, 012028 (2014).

https://doi.org/10.1557/jmr.2014.398 Published online by Cambridge University Press

48. P. Lin, G. Palumbo, U. Erb, and K.T. Aust: Influence of grain boundary character distribution on sensitization and intergranular corrosion of alloy 600. *Scr. Metall. Mater.* **33**, 1387–1392 (1995).
49. P. Lejček: *Grain Boundary Segregation in Metals* (Springer, 2010).
50. S. Watanabe, Y. Takamatsu, N. Sakaguchi, and H. Takahashi: Sink effect of grain boundary on radiation-induced segregation in austenitic stainless steel. *J. Nucl. Mater.* **283–287**(Part 1), 152–156 (2000).
51. R. Hu, G.D.W. Smith, and E.A. Marquis: Effect of grain boundary orientation on radiation-induced segregation in a Fe-15.2 at%Cr alloy. *Acta Mater.* (2013).
52. M. Bachhav, G.R. Odette, and E.A. Marquis: Microstructural changes in a neutron-irradiated Fe–6 at.%Cr alloy. *J. Nucl. Mater.* **453**, 334–339 (2014).
53. S. Mandal, K.G. Pradeep, S. Zaefferer, and D. Raabe: A novel approach to measure grain boundary segregation in bulk polycrystalline materials in dependence of the boundaries' five rotational degrees of freedom. *Scr. Mater.* **81**, 16–19 (2014).
54. M. Herbig, D. Raabe, Y.J. Li, P. Choi, S. Zaefferer, and S. Goto: Atomic-scale quantification of grain boundary segregation in nanocrystalline material. *Phys. Rev. Lett.* **112**, 126103 (2014).
55. M.P. Moody, F. Tang, B. Gault, S.P. Ringer, and J.M. Cairney: Atom probe crystallography: Characterization of grain boundary orientation relationships in nanocrystalline aluminium. *Ultramicroscopy* **111**, 493–499 (2011).
56. V.J. Araullo-Peters, B. Gault, S.L. Shrestha, L. Yao, M.P. Moody, S.P. Ringer, and J.M. Cairney: Atom probe crystallography: Atomic-scale 3-D orientation mapping. *Scr. Mater.* **66**, 907–910 (2012).
57. P. Felfer, A. Ceguerra, S. Ringer, and J. Cairney: Applying computational geometry techniques for advanced feature analysis in atom probe data. *Ultramicroscopy* **132**, 100–106 (2013).
58. M. Bachhav, Y. Chen, E.A. Marquis, and B. Geiser: Measuring chemical segregation at grain boundaries by atom probe tomography. *Microsc. Microanal.* **19**, 940–941 (2013).
59. B.W. Krakauer and D.N. Seidman: Absolute atomic scale measurements of the Gibbsian interfacial excess of solute at internal interfaces. *Phys. Rev. B* **49**, 6724 (1993).
60. B. Gault, F. Danoix, K. Hoummada, D. Mangelinck, and H. Leitner: Impact of directional walk on atom probe microanalysis. *Ultramicroscopy* **113**, 182–191 (2012).
61. T. Toyama, Y. Nozawa, W. Van Renterghem, Y. Matsukawa, M. Hatakeyama, Y. Nagai, A. Al Mazouzi, and S. Van Dyck: Grain boundary segregation in neutron-irradiated 304 stainless steel studied by atom probe tomography. *J. Nucl. Mater.* **425**, 71–75 (2012).
62. A. Etienne, B. Radiguet, N.J. Cunningham, G.R. Odette, and P. Pareige: Atomic scale investigation of radiation-induced segregation in austenitic stainless steels. *J. Nucl. Mater.* **406**, 244–250 (2010).
63. A. Etienne, B. Radiguet, N.J. Cunningham, G.R. Odette, R. Valiev, and P. Pareige: Comparison of radiation-induced segregation in ultrafine-grained and conventional 316 austenitic stainless steels. *Ultramicroscopy* **111**, 659–663 (2011).
64. M.K. Miller, P. Pareige, and M.G. Burke: Understanding pressure vessel steels: An atom probe perspective. *Mater. Charact.* **44**, 235–254 (2000).
65. M.K. Miller: Atom probe tomography characterization of solute segregation to dislocations. *Microsc. Res. Tech.* **69**, 359–365 (2006).
66. C.A. Williams, J.M. Hyde, G.D.W. Smith, and E.A. Marquis: Effects of heavy-ion irradiation on solute segregation to dislocations in oxide-dispersion-strengthened Eurofer 97 steel. *Nucl Mater*. **412**, 105 (2011).
67. A. Bhattacharya, E. Meslin, J. Henry, C. Pareige, B. Décamps, C. Genevois, D. Brimbal, and A. Barbu: Chromium enrichment on the habit plane of dislocation loops in ion-irradiated high-purity Fe–Cr alloys. *Acta Mater.* **78**, 394–403 (2014).
68. S.S. Brenner and D.N. Seidman: Field-ion microscope observations of voids in neutron-irradiated molybdenum. *Radiat. Eff. Defects Solids* **24**, 73–78 (1975).
69. T.J. Godfrey, R.J. Lewis, D.A. Smith, and G.D.W. Smith: On the nature and distribution of defects in tungsten lamp wire. *J. Less-Common Met.* **44**, 319–326 (1976).
70. M.K. Miller, L. Longstreth-Spoor, and K.F. Kelton: Detecting density variations and nanovoids. *Ultramicroscopy* **111**, 469–472 (2011).
71. P.J. Birdseye, D.A. Smith, and G.D.W. Smith: Analogue investigations of electric field distribution and ion trajectories in the field ion microscope. *J. Phys. D: Appl. Phys.* **7**, 1642 (1974).
72. P.D. Edmondson, C.M. Parish, Y. Zhang, A. Hallen, and M.K. Miller: Helium bubble distributions in a nanostructured ferritic alloy. *J. Nucl. Mater.* **434**, 210–216 (2013).
73. J.M. Hyde, M.G. Burke, G.D.W. Smith, P. Styman, H. Swan, and K. Wilford: Uncertainties and assumptions associated with APT and SANS characterisation of irradiation damage in RPV steels. *J. Nucl. Mater.* (2013).
74. I.M. Robertson, C.A. Schuh, J.S. Vetrano, N.D. Browning, D.P. Field, D.J. Jensen, M.K. Miller, I. Baker, D.C. Dunand, R. Dunin-Borkowski, B. Kabius, T. Kelly, S. Lozano-Perez, A. Misra, G.S. Rohrer, A.D. Rollett, M.L. Taheri, G.B. Thompson, M. Uchic, X-L. Wang, and G. Was: Towards an integrated materials characterization toolbox. *J. Mater. Res.* **26**, 1341–1383 (2011).

https://doi.org/10.1557/jmr.2014.398 Published online by Cambridge University Press